UNIVERSITY OF OKLAHOMA

GRADUATE COLLEGE

IMPACTS OF ACOUSTIC WAVES ON THE GAS-LIQUID INTERFACE WITHIN CAPILLARY TUBES

A THESIS

SUBMITTED TO THE GRADUATE FACULTY

in partial fulfillment of the requirements for the

Degree of

MASTER OF SCIENCE

By

JONATHAN J. FLOM
Norman, Oklahoma
2017

IMPACTS OF ACOUSTIC WAVES ON THE GAS-LIQUID INTERFACE WITHIN CAPILLARY TUBES

A THESIS APPROVED FOR THE
MEWBOURNE SCHOOL OF PETROLEUM AND GEOLOGICAL ENGINEERING

BY

_____
Dr. Rouzbeh G. Moghanloo, Chair

_____
Dr. Carl Sondergeld

_____
Dr. Deepak Devegowda

I dedicate this thesis to my parents, Matthew and Nora Flom, whose support through both my Bachelor's and Master's degrees has been indispensable. I would not be where I am today without your love and support.

Thank you

Acknowledgements

First and foremost, I want to acknowledge and thank my advisor, Dr. Rouzbeh Moghanloo, for the constant support and affirmation of my work. Although his knowledge is in a different league than my own, our discussions were always guided by genuine curiosity, and my ideas and insights felt as though they were regarded by an academic peer and not necessarily by a superior. I am thankful that I had the opportunity to not only share the work done on my thesis, but for the many other discussions we have had along the way.

I would also like to thank the many friends I have made through both my undergraduate and master's degrees. I can easily say that I have learned more from the many hours of studying and work we put in together than I could ever have on my own.

Furthermore, I want to thank the faculty and staff of the Petroleum Engineering department and OU. There are too many people and positions to address here, but everyone has contributed to my experience here at OU. The professors especially have sculpted my knowledge, and although it was begrudging at the time, I am thankful for the rigor they imposed upon me. I have constantly been amazed at the amount of material and the pace I have learned throughout the curriculum. Additionally, the various staff in the department who, through all of the complementary organizations and functions they coordinate, have been a consistent pillar of support that I have leaned on to make it year to year.

Finally, I would like to again thank my parents for all of their love and support. There is a reason why I dedicate my Thesis to you both.

Table of Contents

Acknowledgements iv

List of Tables vii

List of Figures viii

Abstract x

Chapter 1: Introduction 1

1.1 Scope of the problem 1

1.2 Research objectives 2

1.3 Chapter summaries 2

Chapter 2: Background and Literature Review 4

2.1 Fundamentals of Contact Angle and Capillary Pressure 4

2.1.1 Interfacial tension and contact angle 4

2.1.2 Capillary pressure within tubes 5

2.2 Gas Condensate Reservoirs 7

2.2.1 Condensate Reservoir Phase Behavior and Condensate Banking 7

2.2.2 Two Phase Flow in the Reservoir and its Relation to Skin 10

2.4 Empirical/Field Studies 12

2.4.1 Seismic irradiation in heavy oil 13

2.4.2 Enhancement during waterflooding 14

2.4.2 General theory of the mechanisms 16

Chapter 3: Methodology 19

3.1 Assumptions 19

3.2 Relating contact angle to curvature radius and capillary tube diameter 20

3.3 Relating acoustic interference and the gas-liquid interface 24
3.3.1 Changes in contact angle 24
3.3.2 Changes in meniscus volume 25
3.3.3 Effect on capillary pressure 25
3.5 Work done by acoustic interference 26
Chapter 4: Simulation 28
4.1 COMSOL Multiphysics® Model 28
4.1.1 Description of Physics Used within COMSOL 28
4.1.2 Description of Model 29
4.1.3 Velocities under varying pressure gradients 33
4.2 Effective Frequencies 36
4.2.1 Approximating likely frequencies 36
4.2.2 Velocities under varying pressure gradients 37
Chapter 5: Conclusions and Future Work 41
5.1 Conclusions 41
References 43
Appendix A: Nomenclature 47

List of Tables

Table 1. Summary of interface movement under various pressure gradients. 36

Table 2. Frequencies in MHz at varying compressional wave velocities 37

Table 3. Frequency dependent displacements after 0.05 seconds under a 10 psi/ft pressure gradient..... 38

Table 4. Summary of interface displacements over 0.05 seconds with ambient pressure waves of 1,800 MHz..... 39

List of Figures

Figure 1. Contact angle exhibited between the gas and liquid phases 4

Figure 2. Contact angle measured from within a capillary tube..... 6

Figure 3. Phase envelope for retrograde gas condensate reservoir (Fan, et al., 2005). 7

Figure 4. Condensate saturation in the near wellbore region (Narayanaswamy, Pope, Sharma, Hwang, & Vaidya, 1999) 9

Figure 5. Pressure profile for a gas condensate well experiencing condensate banking (Fan, et al., 2005)..... 12

Figure 6. Interface model showing small amplitude oscillations (Sohrabi and Jamiolahmady, 2009) 17

Figure 7 - Inverse of capillary tube with defined reference frame 21

Figure 8 - Measure of contact angle according to meniscus effect 23

Figure 9. Representation of capillary tube with two interfaces. 27

Figure 10. Basic schematic of capillary tube. Assumed symmetry with rotation about r = 0 axis..... 30

Figure 11. Physics generated meshing generated within COMSOL 31

Figure 12. Model initialized with gaseous propane in red and liquid heptane in blue... 32

Figure 13. Model of interface with slight movement from initialized point due to non-equilibrium 32

Figure 14. Interface position t = 0 and t = 0.05 seconds under no pressure gradient..... 33

Figure 15. Interface position t = 0 and t = 0.05 seconds under pressure gradient of 2 psi/ft..... 34

Figure 16. Interface position t = 0 and t = 0.05 seconds under pressure gradient of 10 psi/ft 34
Figure 17. Interface position t = 0 and t = 0.05 seconds under pressure gradient of 30 psi/ft 35
Figure 18. Interface position t = 0 and t = 0.05 seconds under pressure gradient of 40 psi/ft 35
Figure 19. Percentage increase of interface displacement after 0.05 seconds at varying frequencies under a 10 psi/ft pressure gradient. 39
Figure 20. Magnitude of interface displacement (Red) and percentage increase of initial displacement (Blue) after 0.05 seconds in the presence of 1,800 MHz pressure waves. 40

Abstract

The focus of this thesis is specifically on the effect that ultrasonic waves have on the interface curvature and subsequent capillary pressure alterations within capillary tubes. In order to optimize current ultrasonic treatments as a means of remediating oilfield complications, such as condensate banking, the exact microphenomena must first be better understood. Many contributing phenomena have been proposed and attributed to observed increases in production during acoustic stimulation, but the focus here in on interface manipulation.

A mathematical model relating changes in curvature to capillary pressure is proposed, and the relationships therein were compared to simulations run using COMSOL Multiphysics®. It was found that under an external pressure gradient, acoustic frequencies increased the interface velocity by up to 18.75% with varying degrees of success under differing pressure gradients. Furthermore, the effective frequency range for a 1.5 μm pore was found to be approximately 750 MHz to 6,000 MHz, and the maximum benefit was observed when a frequency of around 1,800 MHz was applied. In terms of optimizing acoustic treatments, these exceedingly high acoustic frequencies may suggest that other mechanisms should be explored as the main contributors to observed increases in flow.

Chapter 1: Introduction

1.1 Scope of the problem

Gas condensate reservoirs have a tendency to exhibit a phenomenon called condensate banking. The exact mechanisms and ramifications of this phenomenon will be discussed in chapter 2.3, but the existence of condensate as a liquid phase within the near wellbore region can significantly reduce the flow potential in this zone. Furthermore, residual saturations of the heavier components trapped in their liquid phase, which are the more valuable or "sweeter" components, can lead to reduced quality of the production stream (Sayed & Al-Muntasheri, 2016). Many methods have been developed to prevent condensate dropout, mitigate the amount that becomes trapped once condensation occurs, and recover hydrocarbons that have been trapped. These methods have included, but are by no means limited to, using solvents or other chemicals to affect wettability within the reservoir, gas cycling, injection of nitrogen or supercritical CO_2, acidizing, and various other completion techniques targeted at reducing skin or maximizing reservoir contact (Sayed & Al-Muntasheri, 2016). Each have various degrees of benefits and drawbacks and are explained in detail by Sayed and Al-Muntasheri (2016).

Of the many techniques applied in industry, acoustic stimulation is proposed here as a possible alternative. It has the added benefit of not using chemicals that could pose a health or safety concern. Furthermore, it would not generate corrosive substances like carbonic acid from CO_2 injection, and depending on method of implementation, it could allow for continual production during treatment. Finally, targeting effects in the near wellbore region would greatly lower the energy required due to the large attenuation that is experienced as waves propagate further distances into formations. O'Connell and

Budiansky (1977) have shown how great attenuation of elastic waves can be through their evaluation of wave propagation in the presence of fluid filled cracks. In their work, they identified two conditions under which the attenuation was largest: fluid flow between cracks and shear stress relaxation in an isolated viscous fluid inclusion O'Connell and Budiansky (1977).

1.2 Research objectives

Although empirical evidence has shown positive effects on the flow of oil while in the presence of acoustic stimulation, which is discussed in greater detail in chapter 2.4, the exact micro-phenomena regarding the causes of observed productivity increases are not yet well defined. One dominant theory attributes these empirical increases in liquid mobility to poroelastic deformation of the rock matrix. Others attribute these increases to decreased fluid viscosities, destabilization of fluid adherence to wall surfaces, coalescence of oil droplets, and alterations to local pressure gradients within the reservoir (Zhu, Huang, & Vajjha, 2005). This thesis explores and attempts to better define the competing phenomena whereby capillary pressure is affected from changes in interface curvature. If this mechanism were to play a significant role in production increase, it would need to be taken into account for treatment optimization.

1.3 Chapter summaries

Chapter 2 gives background knowledge required to understand some of the mechanisms involved with this evaluation. The meniscus within capillary tubes is explained through the relationship between interfacial tension and the resulting surface

wetting. The curvature created through wettability is used to describe the magnitude of pressure difference between the phases, which is described as capillary pressure. Additionally, Chapter 2 explains the phase behavior of gas condensate reservoirs and the process of developing a condensate bank near the wellbore where the reservoir pressure drops below the dewpoint.

Chapter 3 derives the mathematical expression relating acoustic interference to interface displacement and subsequent effects on capillary pressure. Assuming no-slip boundaries, the maximum interface displacement would be in the center of the capillary tube. This results in an induced curvature change in the interface. Through the derived expression, this intimates that the energy propagated by the acoustic goes towards moving the interface and adjusting the resulting capillary pressures.

Chapter 4 discusses and summarizes simulations using COMSOL Multiphysics®. Various pressure gradients and frequencies were simulated on a 1.5 μm tube, and increases in net interface displacement and velocities were observed.

Chapter 5 highlights some of the important conclusions from chapters 3 and 4, and summarizes the findings as well.

Chapter 2: Background and Literature Review

In order to understand how sound waves interact with multiphase flow within capillary tubes, some basic understanding of interfacial tension and capillary pressures must first be established. The following sections discuss the role of interfacial tension and the resulting surface wetting that occurs in capillary tubes to the definition of capillary pressure itself. Also discussed here are results from experiments and field application with current hypotheses for increased flow contribution due to acoustic stimulation.

2.1 Fundamentals of Contact Angle and Capillary Pressure

2.1.1 Interfacial tension and contact angle

Due to cohesive properties between particles in their liquid phase, a disparity in forces is created when there is an interface between them and particles with different internal cohesive forces. This manifests as surface tension, where the particles exhibit stronger attractions to each like particle along the plane of the interface rather than to the apposing fluid. This disparity leads the fluid with greater cohesive forces to minimize the surface area in contact with the other fluid. The resulting sphericity is dependent on the magnitude of the disparity in forces, with larger disparities exhibiting more spherical behavior. When in contact with a solid surface, there exists an angle whereby the cohesive fluid partially exhibits its desired spherical nature, which can be seen in **Fig. 1**.

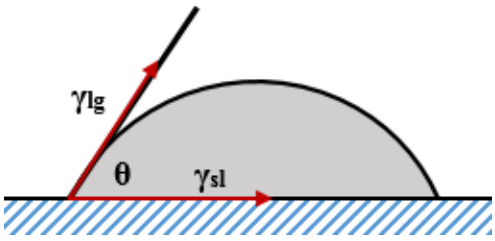

Figure 1. Contact angle exhibited between the gas and liquid phases

The contact angle, denoted by θ, is measured from the solid-liquid interface, γ_{sl}, to the liquid-gas interface, γ_{lg}. This angle is due to the cohesive forces of the fluids as well as the physical properties of the solid surfaces, such as composition and roughness. These factors lead to defining wettability, which is the liquid's tendency to coat the solid surface when in the presence of another phase. In Fig. 1 above, the liquid represents the wetting fluid, or the fluid having the greater tendency to coat the solid surface. Between two liquids, like with water and oil, one may be considered wetting due to certain solid-liquid interactions and the other may be wetting with differing interactions.

Although the wetting interactions between solid surfaces and both oil and water are very important in relating flow in porous media, the work done in this thesis look more specifically at the interaction between oil or condensate as the wetting phase with natural gas as the non-wetting phase.

2.1.2 Capillary pressure within tubes

As a result of the interfacial tension and wettability, liquids within capillary tubes will develop a meniscus at the interface. This effect is shown in **Fig. 2** along with the corresponding measure of contact angle.

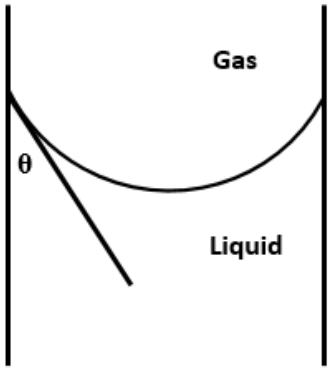

Figure 2. Contact angle measured from within a capillary tube

The severity of the curvature is related to the factors affecting interfacial tension and wettability but is also dependent on the radius of the capillary tube. The disparity in forces leads to differing internal pressures between, in this case, the liquid and gaseous phases. Capillary pressure, or P_c, is defined as the difference between the internal pressure of the non-wetting and the wetting phases, which is represented below as **Eq. 2.1**.

$$P_c = P_{non-wet} - P_{wet} \tag{2.1}$$

Capillary pressure, thus, is a function of the interfacial tension, the radius of the capillary tube, and the contact angle exhibited between the phases and the solid surface. This relationship is defined through the Young–Laplace equation, given as **Eq 2.2**, with γ being the interfacial tension and R being the radius of the capillary tube.

$$P_c = \frac{2\gamma \cos(\theta)}{R} \tag{2.2}$$

Capillary forces have little impact on flow within sufficiently large pipes, but they become increasingly important when dealing with smaller tubes, like those exhibited within porous media.

2.2 Gas Condensate Reservoirs

2.2.1 Condensate Reservoir Phase Behavior and Condensate Banking

Gas condensate, or retrograde-gas, reservoirs contain hydrocarbons with average molecular weights between those of wet gas and volatile oil reservoirs. Their distribution of hydrocarbons leads gas condensate reservoirs to initially begin as a single-phase gas in the reservoir, but unlike wet gas reservoirs, isothermal pressure depletion eventually leads to crossing the dewpoint line on the pressure versus temperature phase diagram (McCain, 1990) shown below in **Fig. 3** by (Fan, et al., 2005).

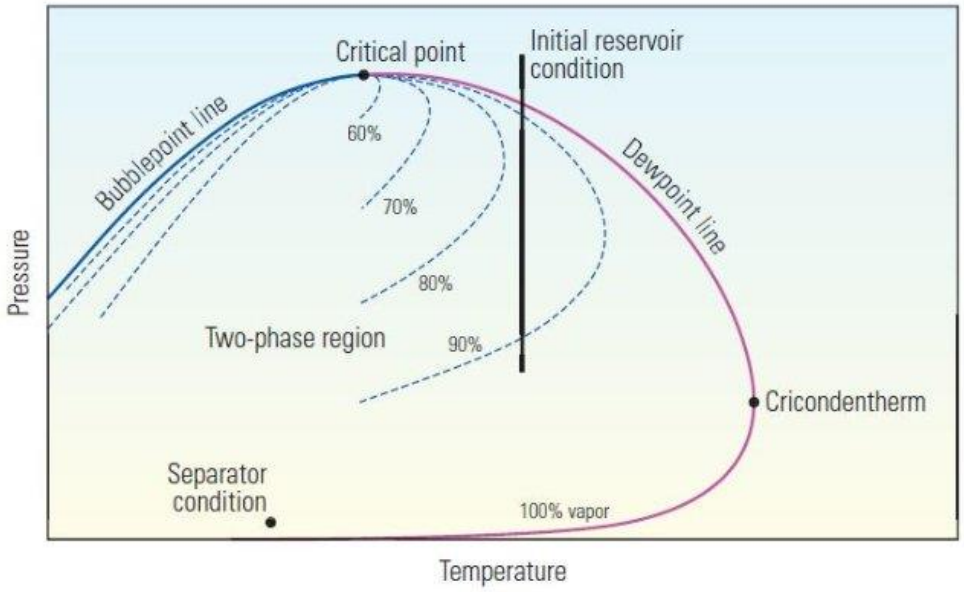

Figure 3. Phase envelope for retrograde gas condensate reservoir (Fan, et al., 2005).

Once the reservoir crosses the dewpoint line, the existing pressure and temperature conditions no longer support molecular kinetic energies great enough to overcome the intermolecular forces. As a result, the hydrocarbon molecules coalesce into a liquid phase where the molecular interaction is dominated by the intermolecular forces.

This typically occurs first with the heavier components due to the higher molecular weights of the longer hydrocarbon chains (McCain, 1990).

As the pressure continues to deplete, the existing reservoir conditions continue further into the two-phase region of the phase envelope, and the ratio of components in the liquid phase proportionally increase compared to those of the gas. Although it can be seen that pressure depletion on the far right of the phase envelope, near the cricondentherm, may eventually lead back into the single-phase gas region at sufficiently low pressures, this phenomenon is unlikely to occur in the field (McCain, 1990).

The lowest pressure in a reservoir, and subsequently the most likely place to first enter the two phase region, is near the wellbore. As a result, the near wellbore region of a gas condensate reservoir tends to develop a repository of condensate, which is referred to as condensate banking. A simulated reservoir showing the condensate banking phenomenon can be seen below in **Fig. 4** (Narayanaswamy et al., 1999). It can be clearly seen that the condensate is concentrated almost exclusively to the near wellbore region. The upper portion of the reservoir was simulated with greater permeability, which allows for a greater pressure gradient reaching into the formation. This greater pressure gradient is responsible for the condensate bank reaching further into the reservoir (Narayanaswamy et al., 1999).

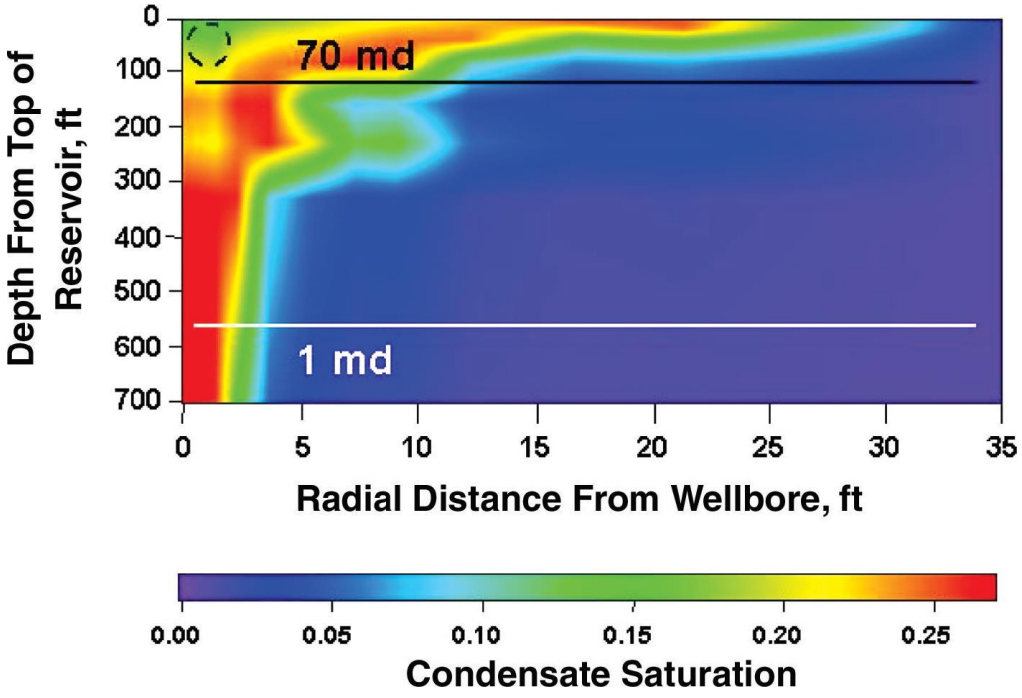

Figure 4. Condensate saturation in the near wellbore region (Narayanaswamy, Pope, Sharma, Hwang, & Vaidya, 1999)

This banking is described in further detail by Marokane et al. (2002) and Sayed and Al-Muntasheri (2016) who explained four distinct regions of the condensate bank, which are listed and described below.

1. Region furthest from the wellbore where reservoir pressure is above the dewpoint and is exhibits single-phase flow
2. Region with condensate saturation below residual saturation. In this region, the condensate is immobile, and the flow still exists as single-phase.
3. Region with increased condensate saturation above critical saturation. In this region, two-phase flow exists.
4. Region directly adjacent to the wellbore where sufficiently high gas flow rates slightly increase liquid flow due to velocity stripping.

2.2.2 Two Phase Flow in the Reservoir and its Relation to Skin

Once there exists both gas and liquid phases, the flow potential in the reservoir is greatly changed, and the flow preferentially lends itself to the gaseous phase over that of the liquid. Although the tendencies of the denser phase towards wetting the solid surface play a role as to why gas preferentially flows over liquid, another dominating factor in this case is the difference in viscosity between the phases. This effect is clearly illustrated by taking the ratio of the gas to liquid flow rate correlated through Darcy's Law, with Darcy's Law being **Eq 2.3** below.

$$q = \frac{kA}{\mu}\frac{dP}{dx} \tag{2.3}$$

Under the same pressure gradient flowing through the same cross-sectional area, the ratio of the flow of gas over liquid is directly related to the permeabilities of each phase and their respective viscosities, which can be seen in **Eq. 2.4**.

$$\frac{q_g}{q_l} = \frac{k_g \mu_l}{k_l \mu_g} \tag{2.4}$$

The viscosities of gasses and liquids vary greatly with pressure, temperature, and composition, but the difference between the viscosities of natural gas and oils can be orders of magnitude different with gas being significantly less viscous (Coats & Smart, 1986). This, along with differences in permeability between the phases and the capillary forces, significantly increases potential for gaseous flow over liquid.

Due to the phenomenon of condensate banking, this decreased mobility of the liquid phase from viscosities and capillary forces occurs in the near wellbore region, most significantly in the aforementioned regions 2, 3, and 4 described by Marokane et al.

(2002) and Sayed and Al-Muntasheri (2016). In addition to the economic considerations of losing the heavier and more costly hydrocarbons due to residual saturations (Sayed & Al-Muntasheri, 2016), there can exist significant alterations to the flow potential and productivity of the reservoir, with the productivity index relationship described below as **Eq. 2.5**.

$$J = \frac{q}{P_{res} - P_{wf}}; \qquad J \alpha \frac{1}{s} \tag{2.5}$$

In the above equation, P_{res} and P_{wf} are the reservoir and wellbore pressures respectively, and q is the flow rate induced from the difference in these pressures. J represents the productivity index and is related to properties such as permeability, viscosity, formation volume factor, reservoir thickness, wellbore configuration, and skin (Economides et al., 2016). The important relationship, however, is the inverse relationship between skin and productivity index because the losses in productivity due to condensate banking may be correlated to an effective two-phase skin. Raghavan et al. (1999) proposes a means of quantifying this negative effect on productivity through correlations for skin using well testing.

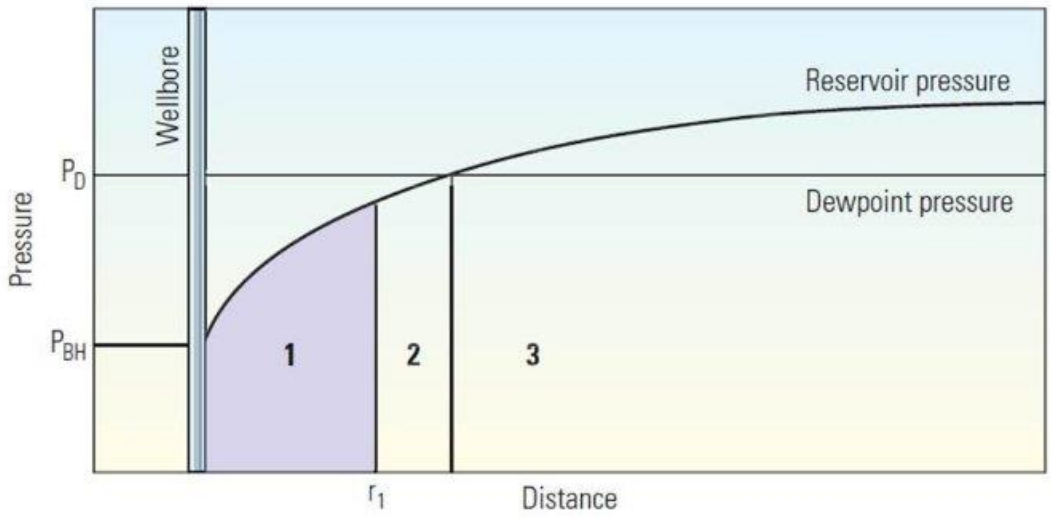

Figure 5. Pressure profile for a gas condensate well experiencing condensate banking (Fan, et al., 2005).

Figure 5 (Fan, et al., 2005) shows pressure as a function of distance from the wellbore for a condensate banking system. Region 3 in this figure represents the above dewpoint region, Region 2 is subcritical condensate saturation with single phase flow, and Region 1 represents the region where condensate saturation is above critical levels and where two phase flow exists. It should be noted that the largest changes in pressure are exhibited between the above Regions 1 and 2, which represent the two phase regions.

2.4 Empirical/Field Studies

Much of the study and application of acoustic stimulation has been done in regards to increasing the efficiency of waterflooding with various other applications including heavy oils in China. To understand the potential applicability to gas condensate reservoirs, various experiments and field applications have been evaluated, and the proposed mechanisms are discussed in the following sections.

2.4.1 Seismic irradiation in heavy oil

Vibration and ultrasonic based stimulation have been implemented successfully in a variety of field applications, many of which have targeted improving oil recovery during waterflooding or in reservoirs with heavy oil. Zhu et al. (2005) describes a few studies where vibration based stimulation successfully increased production in Liaohe, Huabei, and Shengli oilfields, among others. The downhole vibration system created 88 high amplitude shocks per minute. When the tool was implemented in the Liaohe field, which produces from a high permeability reservoir with heavy oil that was previously in late cyclic steam stimulation, there was an increase of 47.6% oil production with a decrease in water cut from 63% down to 58%. Not only was this treatment effective in the well from which the tool was placed, but nearby wells also experienced increases in oil production, with one in particular that experienced a 400% increase in production (Zhu et al., 2005).

When the treatment was applied in the Huabei field, which is a low-permeability reservoir when compared to the high permeability Liaohe, 58 wells surrounding the source of vibration experienced increases in production. The average production increase experienced was 27.5% with reductions in water oil ratio (WOR) ranging from 10% to 75% (Zhu, Huang, & Vajjha, 2005). It should be noted, though, that the vibration source emitted seismic waves whose wavelengths were well below ultrasonic frequencies discussed in this thesis. In contrast to the proposed effect on capillary pressure, the describing phenomena leading to these massive increases were attributed in these studies to large decreases in viscosities from shearing forces in these heavier oil reservoirs.

2.4.2 Enhancement during waterflooding

Many experiments, both in the lab and field trials, have shown improvements to waterflooding when acoustic stimulation has been implemented. Mohammadian et al. (2013) designed a sand pack experiment where Kerosene, Vaseline, and engine oil were tested as the non-wetting phase. Within the unconsolidated system, increases of 3-16% total oil recovery were observed when stimulated with ultrasonic irradiation. They proposed emulsification and cavitation as the likely mechanisms that lead to the observed increases (Mohammadian et al., 2013). Naderi and Babadagli (2010) performed experiments on a sandstone core placed within an imbibition cell. Frequencies from 22 to 40 kHz were applied, and in every test, oil recovery increased as compared to the base recovery without acoustic interference.

In core flooding experiments performed by Alhomadhi et al. (2014) on Barea sandstone saturated with Saudi crude oil, ultimate oil recovery was increased from 54% to 59% in horizontal core floods while vertical core floods increased from 49.9% to 58% when ultrasonic frequencies of 50 kHz where applied. They also noted that although water saturations within the core were ultimately lower, water breakthrough happened earlier in the horizontal core floods and later in the vertical core floods. They attributed these effects of increased production with varying degrees of breakthrough to increased gravitational separation, which led them to suggest that ultrasonic irradiation during waterflooding might be more effective in horizontal wells (Alhomadhi et al., 2014).

Kouznetsov et al. (1998) discussed both laboratory tests as well as field trials of vibro-seismic irradiation with frequencies in the range of 100 to 200 Hz. In two separate

experiments on kerosene saturated sandstone cores, they observed 32% oil recovery after 300 hours for direct-flow capillary saturation and 56% recovery after 325 hours for inverse-flow capillary saturation. After the elastic waves were applied, the recoveries increased to 60% after 51 hours and 96% after 92 hours for the two cases. When the same frequencies were applied in field examples, the water cuts in both the Abuzy and Changirtash oilfields decreased by 20-26% and 25-30%. Kouznetsov et al. (1998) suggested three proposed mechanisms for these experimental and field results:

1. Periodic movements of the two liquid phases lessens their adherence to the pore walls, and due to the relative densities of oil and water, oil will experience greater acceleration than water.
2. The periodic movements break apart water films within the reservoir that block oil flow through the more narrow pores, leading to increases in the relative permeability to both phases.
3. Reductions in the interfacial tension and contact angle between the phases leads to increased relative permeability specifically to oil over water.

Abramov et al. (2013) evaluated and described field implementation of ultrasonic stimulation in failing wells. In these field studies, a downhole tool emitted ultrasonic waves in both temporary and permanent applications. It was noted that wells in reservoirs above 15% porosity and greater than 20 mD experienced increases in oil production by up to 50% or more while wells with lower permeability or porosity were not as successful (Abramov et al., 2013).

2.4.2 General theory of the mechanisms

In addition to the many mechanisms addressed above, one other significant mechanism proposed is the contribution from pore deformation. The idea was initially proposed by Ganiev et al. (1989) who suggested the pore deformation would be caused by travelling transversal waves, and that this deformation would lead to increases in flow. The idea was later refined by Aarts and Ooms (1989) and Aarts et al. (1999) who demonstrated strong influences from both fluid compressibility and pore wall hardness. Furthermore, Aarts et al. (1999) went on to show how this version of "peristaltic transport" is only effective at ultrasonic frequencies, and that the effective range would be limited to near the wellbore due to large attenuation.

Although briefly mentioned by Kouznetsov et al. (1998), Sohrabi and Jamiolahmady (2009) goes into detail in describing the possible implications that ultrasonic waves have on the interface and interface displacement. They performed experiments on a 1 mm glass capillary tube as well as a modeled network of acid etched glass capillary tubes. With the application of 20 kHz ultrasonic waves, Sohrabi and Jamiolahmady (2009) showed thinning of the interface between the phases as well as a net movement in the direction of the less dense phase as the interface oscillates. Assuming no change in curvature of the interface, Sohrabi and Jamiolahmady (2009) derived **Eq. 2.6** below based on **Fig. 6** and showed that there is a net force on the interface in the direction of the less dense phase.

$$F = \pi k P_A R_o^2 R_{\varepsilon o} \sin(\nu) \tag{2.6}$$

Where F is the force in the direction of propagation, k is the wave number and is equal to $2\pi/\lambda$, P_A is the acoustic pressure, R_o is the radius of curvature, $R_{\varepsilon o}$ is the amplitude of radius movement, and ν is the phase factor.

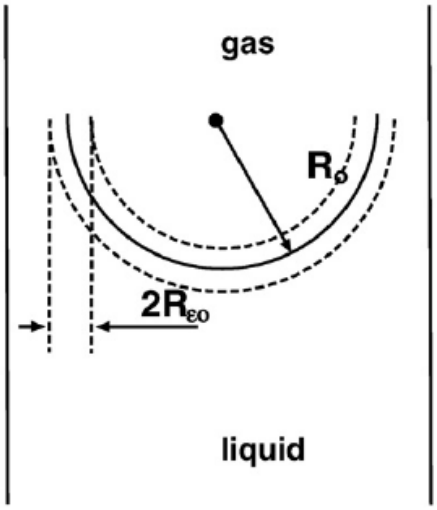

Figure 6. Interface model showing small amplitude oscillations (Sohrabi and Jamiolahmady, 2009)

To summarize the field observations and theoretical review, the following mechanisms all have implications in causing increases in oil production due to elastic wave propagation:

- Poroelastic deformation
- Decreases in fluid viscosity
- Emulsification and cavitation
- Increased gravitational separation
- Effects of periodic motion of the fluids
- Lessening fluid adherence to pore walls
- Interface destabilization

- Changes in capillary pressures.

In order to better optimize field treatments, the effects and relative contributions of each must be evaluated. For the purposes of this thesis, the effect of ultrasonic waves on interfacial tension, contact angle, and capillary pressure are evaluated through chapters 3 and 4.

Chapter 3: Methodology

This section proposes a mathematical derivation relating the work applied from acoustic stimulation to the effects on capillary pressure through changes in interface displacement.

3.1 Assumptions

In order to understand how the following mathematical model was derived, as well as understanding its limitations and shortcoming, a general list of the assumptions is given below.

- Immiscible phase distinction with no exchange of components. Although this is clearly not what exists in a reservoir, it needs to be assumed in order to evaluate the specific work done on changing capillary pressures.
- Negligible work done on stretching the interface during periods of oscillation.
- The interface movement does not experience a hysteresis effect.
- Constant interface curvature with a no-slip boundary during interface movement.
- Incompressible matrix with no tube deformation and negligible liquid compressibility.
- Negligible interface thickness compared to pore diameter.
- Linear acoustic propagation parallel to the capillary tube and the direction of flow.
- Negligible phase shift between acoustic waves and observed interface behavior. Additionally, assumed no interaction between waves in terms of constructive and destructive.

- The system exists in local equilibrium, or Local Equilibrium Assumption (LEA).

Two of these assumptions in particular must first be addressed. For the following derivation, the two phases were assumed to be independent of each other with a clear distinction between the two. The phenomena of condensate banking occurs due to exchanges taking place within the two-phase region. Realistically, there would definitely be some exchange between the phases, but it is assumed here that the majority of phase exchange exists as liquid dropping out creating additional blocked pore throats.

Furthermore, the work done by stretching the interface is assumed to be negligible compared to the amount of energy going towards moving the interface itself. This neglected work is consumed as the particles along the interface are cyclically stretched away from each other and then compressed together. The actual work and interfacial energy associated with the interfacial tension is described in greater detail by Bonn et al. (2009), but for the purposes of this derivation, the differences in work from interface stretching done as two balanced interfaces move through compressional and extensional cycles is assumed to consume less than the displacement itself.

3.2 Relating contact angle to curvature radius and capillary tube diameter

The first step in describing the equation relating the work imposed on moving the gas-condensate interface begins with relating the contact angle to both the capillary tube diameter and the radius of curvature associated with the meniscus. This relation is first defined through system described by **Fig. 7**.

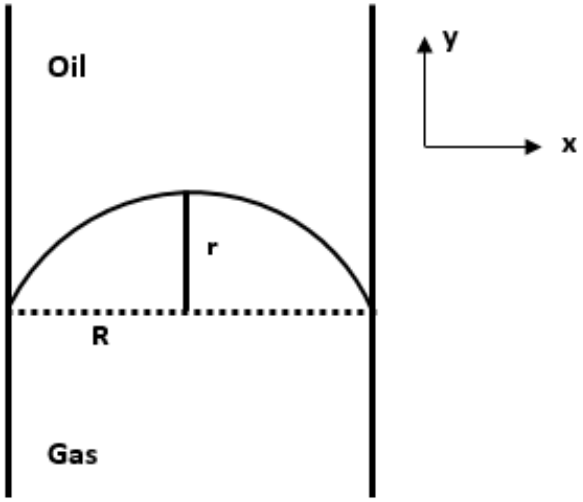

Figure 7 - Inverse of capillary tube with defined reference frame

A constant curvature is assumed across the interface, and the second derivative of its position is set equal to constant a in **Eq. 3.1**.

$$\frac{\partial^2 y}{\partial x^2} = a \tag{3.1}$$

This is then integrated twice over the displacement in the x direction to get **Eq. 3.2 and 3.3** below with Eq. 3.2 describing the slope and Eq. 3.3 describing the position. As a result of the system being defined with the point of contact at (0, 0), the additional integration constant for the position function is 0.

$$\frac{dy}{dx} = ax + b \tag{3.2}$$

$$y = \frac{1}{2}ax^2 + bx \tag{3.3}$$

According the reference frame given in **Fig. 7**, the following conditions describing the position of the interface are given.

$$@x = 0; \qquad y = 0, \qquad \frac{dy}{dx} = b$$

$$@x = R; \qquad y = r, \qquad \frac{dy}{dx} = 0$$

$$@x = 2R; \qquad y = 0, \qquad \frac{dy}{dx} = -\frac{dy}{dx}\Big|_{x=0}$$

At x = R, the first derivative is equal to 0, as shown in **Eq. 3.4** below.

$$aR + b = 0 \tag{3.4}$$

After solving for b, the term is inserted into the position function, which can be seen below in **Eq. 3.5**.

$$y = \frac{1}{2}ax^2 - (aR)x \tag{3.5}$$

At x = R and y = r, this simplifies to;

$$r = -\frac{1}{2}aR^2 \tag{3.6}$$

Giving us the constant a as a function of tube diameter and the maximum displacement;

$$a = \frac{-2r}{R^2} \tag{3.7}$$

At x = 0, the displacement in the y direction is 0, resulting in the first derivative being equal to b. Due to the assumption of constant curvature, the first derivative at x = 2R is equal to the negative derivative at x = 0. By inserting the constant a into the first derivative and equating the derivatives at each boundary, **Eq. 3.8** is given below.

$$\frac{dy}{dx}\Big|_{x=2R} = -b = \frac{-2r}{R^2}x + b \tag{3.8}$$

After simplifying, the constant b is determined as a function of r and R.

$$b = \frac{2r}{R} \tag{3.9}$$

By combining these constants with the position function and its derivatives, we develop **Eq. 3.10 to 3.12** below.

$$\frac{\partial^2 y}{\partial x^2} = \frac{-2r}{R^2} \tag{3.10}$$

$$\frac{dy}{dx} = \frac{-2r}{R^2}x + \frac{2r}{R} \tag{3.11}$$

$$y = \frac{-r}{R^2}x^2 + \frac{2r}{R}x \tag{3.12}$$

The second derivative is of special importance to relating the contact angle to r and R. At the boundary where the contact angle is defined, the derivative is equal constant b. Due to how the contact angle is defined through the wetting fluid, this slope is actually measuring the complementary angle to the contact angle.

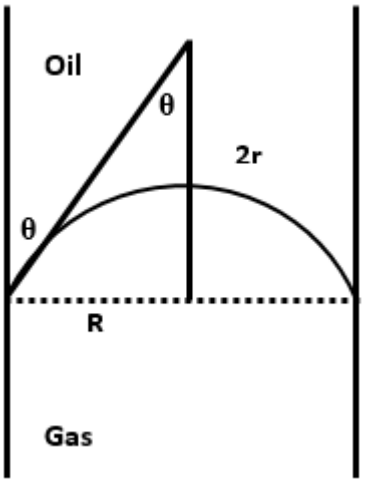

Figure 8 - Measure of contact angle according to meniscus effect

This relation between the slope and the contact angle is given below as **Eq. 3.13**.

$$\theta(r,R) = \tan^{-1}\left(\frac{R}{2r}\right) \tag{3.13}$$

3.3 Relating acoustic interference and the gas-liquid interface

3.3.1 Changes in contact angle

The cyclic nature of the local high and low pressure deviations should prompt interference on the interface between the liquid and gaseous phases. In an idealized system, the amplitude of particle displacement can be modeled by **Eq. 3.14** below.

$$d(t) = r'\cos(kr_x - \omega t + \varphi_d) \tag{3.14}$$

In these equations, r represents radius of curvature, k is the wavenumber, which is equal to $\frac{2\pi}{\lambda}$ with λ being the wavelength, ω is the angular frequency, t is time, and φ is the phase shift. The prime term in each represents the amplitude of variations, and the x subscript represents the unperturbed radius. Of special importance is the radius displacement as a function of time. The actual position of the radius as a function of time is the unperturbed radius plus the amplitude of displacement variations. By assuming no phase shift between the interface displacement and the sound wave oscillations, and after inserting in $\frac{2\pi}{\lambda}$ for k, Eq. 3.14 becomes **Eq. 3.15** below.

$$r(t) = r_x + r'\cos\left(\frac{2\pi}{\lambda} r_x - \omega t\right) \tag{3.15}$$

Assuming a no-slip boundary, the above equation for meniscus radius as a function of time is combined with Eq. 3.13 to get the contact angle as a function of time, seen below as **Eq. 3.16**.

$$\theta(t) = \tan^{-1}\left(\frac{R}{2r_x + 2r'\cos\left(\frac{2\pi}{\lambda}r_x - \omega t\right)}\right) \tag{3.16}$$

3.3.2 Changes in meniscus volume

As the radius of the meniscus changes due to acoustic interference, there is a net volume displacement. This can be modeled by the volume of an ellipsoid, given below as **Eq. 3.17** with x, y, and z being typical Cartesian coordinates.

$$V = \frac{4}{3}\pi xyz \tag{3.17}$$

In the case of a capillary tube with a meniscus the y and z directions represent the tube radius, and the third dimension is the radius of interface curvature, which is related to time using **Eq. 3.18**.

$$\frac{2\pi}{3}R^2\left(r_x + r'\cos\left(\frac{2\pi}{\lambda}r_x - \omega t\right)\right) \tag{3.18}$$

3.3.3 Effect on capillary pressure

By combining the contact angle as a function of time, or Eq. 3.16, with Eq. 2.2, we get **Eq. 3.19** below.

$$P_c = \frac{2\gamma}{R}\cos\left(\tan^{-1}\left(\frac{R}{2r_x + 2r'\cos\left(\frac{2\pi}{\lambda}r_x - \omega t\right)}\right)\right) \tag{3.19}$$

The total pressure drop in the system is defined in this context as the sum of the pressure differences caused by the capillary forces as well as the external ambient pressure difference in the system, as denoted by ΔP_{ext}.

$$\Delta P_T = P_c + \Delta P_{ext} \tag{3.20}$$

By inserting Eq. 3.19 into the above equation, we get **Eq. 3.21.**

$$\Delta P_T = \frac{2\gamma}{R}\cos\left(\tan^{-1}\left(\frac{R}{2r_x + 2r'\cos\left(\frac{2\pi}{\lambda}r_x - \omega t\right)}\right)\right) + \Delta P_{ext} \tag{3.21}$$

The above equation is now the total pressure drop across the interface as a function of time related through acoustic interference.

3.5 Work done by acoustic interference

Work can be described in many, one of which is pressure multiplied by volume. The work done by acoustic waves on the interface can be related by the net effect on capillary pressure through Eq. 3.21, to the change in volume of the ellipsoid through Eq. 3.18. The resulting relationship is given below as **Eq. 3.22**.

$$PV = \frac{2\pi}{3}R^2\left(r_x + r'\cos\left(\frac{2\pi}{\lambda}r_x - \omega t\right)\right)\left[\frac{2\gamma}{R}\cos\left(\tan^{-1}\left(\frac{R}{2r_x + 2r'\cos\left(\frac{2\pi}{\lambda}r_x - \omega t\right)}\right)\right) + \Delta P_{ext}\right] \tag{3.22}$$

When the displacement term, or the term related through Eq. 3.14, is negative, the effective radius of curvature decreases. During this period, the capillary pressure also decreases, and the energy induced into the system from the acoustic waves goes towards

reducing the difference in wetting and non-wetting pressures. The opposite is true as the effective curvature radius increases. During this period, the capillary pressures are exaggerated, and the energy induced by the compressional waves goes towards increasing the pressure difference between the phases. Due to the cyclic nature of compressional waves, one complete cycle will be defined here as interface displacement from the neutral point through positive, through negative, and back to neutral, which can be seen in **Fig. 9** below.

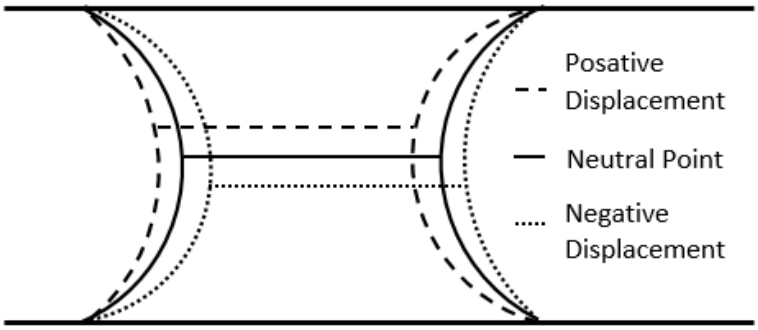

Figure 9. Representation of capillary tube with two interfaces.

If the length of capillary tube is small enough such that the attenuation between interfaces is negligible and under no external pressure gradient, the net work performed by moving the interface through one complete cycle would be zero. However, if there is an ambient pressure gradient, as one would expect with a flowing well, less work would be required to move the interfaces in the direction of lower pressure. If continuous energy is being provided equally to each interface by the acoustic waves, the extra energy during the period of positive displacement would translate to a larger volume displacement in that direction. With repeated cycles, there will be a net increase in flow in the direction of lower pressure gradient strictly due to the acoustic interference.

Chapter 4: Simulation

4.1 COMSOL Multiphysics® Model

COMSOL Multiphysics® was used in the process of validating the proposed effect that sound waves have specifically on the interface between gas and condensate within capillary tubes. COMSOL is a robust numerical simulation software that allows for the coupling of many physics into one model. The numerical process used is based on the finite element method. For the purposes of this study, simulated acoustics were modeled within the computational fluid dynamics module in order to combine the capillary phenomena within the presence of an acoustic field.

4.1.1 Description of Physics Used within COMSOL

Based on the level set approach used in COMSOL, the transport of the fluid interface is modeled using **Eq. 4.1** below (Capillary Filling - Level Set Method). ϕ represents the phase with $\phi = 0$ being for the gaseous phase and $\phi = 1$ for the liquid. ε represents the thickness of the interface, and γ_i is a parameter that determines the amount of initialization, both of which are defined within the simulation itself.

$$\frac{d\phi}{dt} + u \cdot \nabla\phi = \gamma_i \nabla \cdot \left(\varepsilon\nabla\phi - \phi(1-\phi)\frac{\nabla\phi}{|\nabla\phi|}\right) \tag{4.1}$$

In terms of the mass and momentum transport within the capillary tube, Navier-Stokes equations were used (Capillary Filling - Level Set Method). **Eq. 4.2** represents the Navier-Stokes equation taking into account capillary forces and surface tension.

$$\rho\frac{du}{dt} + \rho(u \cdot \nabla)\mathrm{u} = \nabla \cdot \left(-p\mathbf{I} + \mu(\nabla\mathrm{u} + (\nabla\mathrm{u})^T)\right) + F_{st} + \rho g \tag{4.2}$$

Where,

$$F_{st} = \nabla \cdot \mathrm{T} \tag{4.3}$$

$$T = \sigma(\mathbf{I} - \boldsymbol{nn}^{\boldsymbol{T}})\delta \quad (4.4)$$

In the above equations, ρ represents the density, μ is the dynamic viscosity, u is the velocity, p denotes the pressure, g is the gravity, F_{st} is the surface tension acting between the liquid and gaseous phase, I is the identity matrix, n is the interface normal, σ is a surface tension coefficient, δ is a Dirac delta function (Capillary Filling - Level Set Method).

When defining slippage of the interface, COMSOL uses **Eq. 4.5** below.

$$F_{fr} = -\frac{\mu}{\beta}u \quad (4.5)$$

Where F_{fr} is the frictional boundary force and β is the slip length.

4.1.2 Description of Model

The basic schematic of the model used in these simulations can be seen below as **Fig. 9**. A capillary tube with a radius of 1.5 μm and a total length of 200 μm was modeled. The bottom 50 μm and top 100 μm were initialized with pure propane acting as the gaseous phase while the middle 50 μm was initialized with pure Heptane acting as the liquid phase. Due to an assumed symmetry within the capillary tube, the model was designed as a rectangle that is rotated about the r = 0 axis. The ambient temperature and pressures were set at 70℉ and 100 psi. respectively. The inlet is specified at the bottom of the model and the outlet at the top.

Realistically, condensate reservoirs contain a spectrum of hydrocarbon components, and they exist at much higher pressures and temperatures than the above description, but justification of the existence of this interface based phenomenon requires each fluid stay within their respective phases.

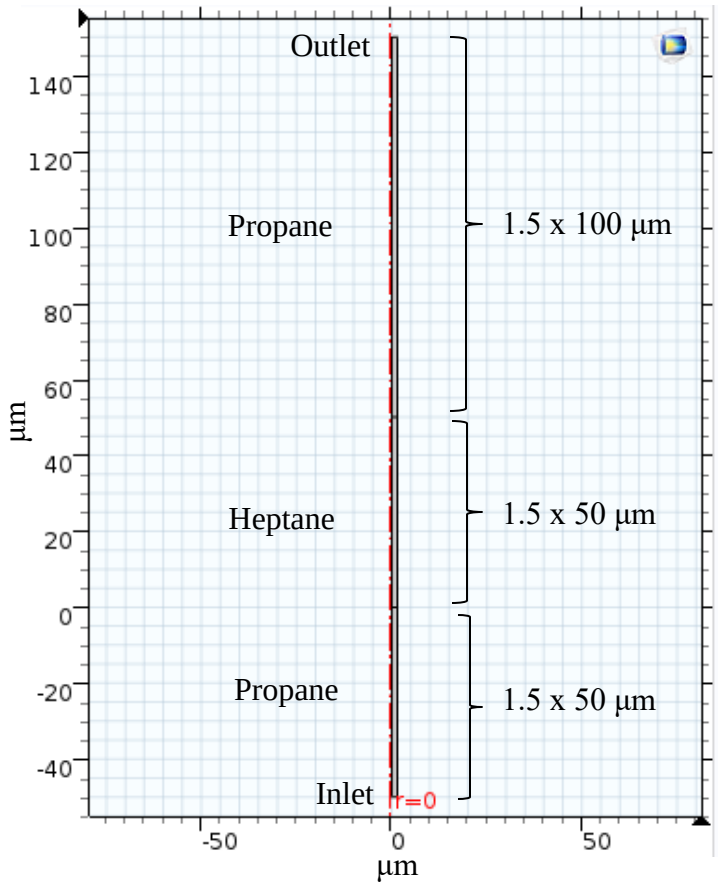

Figure 10. Basic schematic of capillary tube. Assumed symmetry with rotation about r = 0 axis.

The meshing for the finite element method was generated within COMSOL itself and was refined according an internally defined normal coarseness based on the physics implemented. The resulting mesh for this model can be see below as **Fig. 11.**

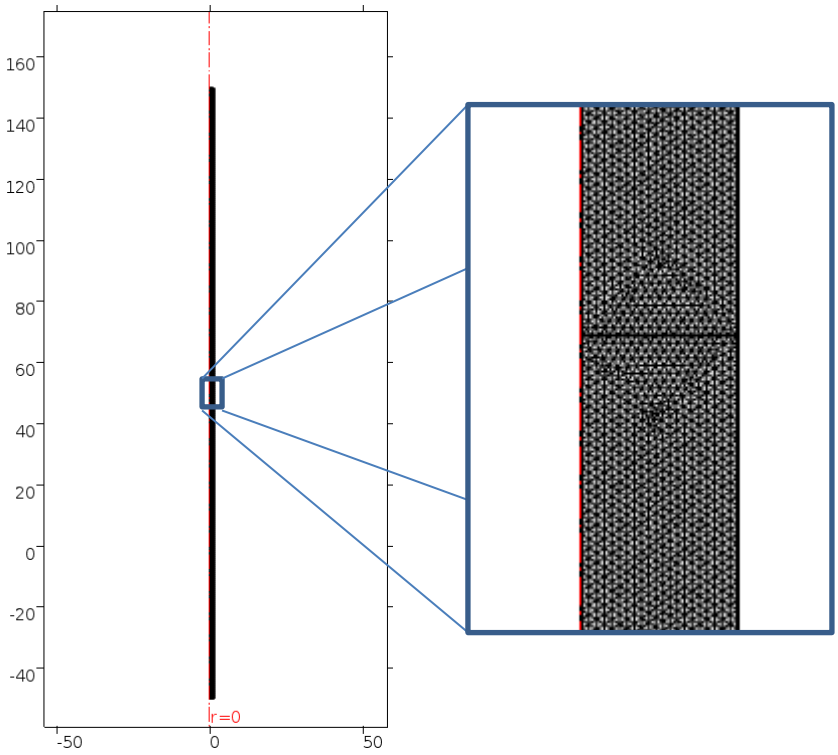

Figure 11. Physics generated meshing generated within COMSOL

The revolved 3D model with the phases initialized in their respective regions can be seen below in **Fig. 12**, and the curvature of the interface can be seen in **Fig. 13**.

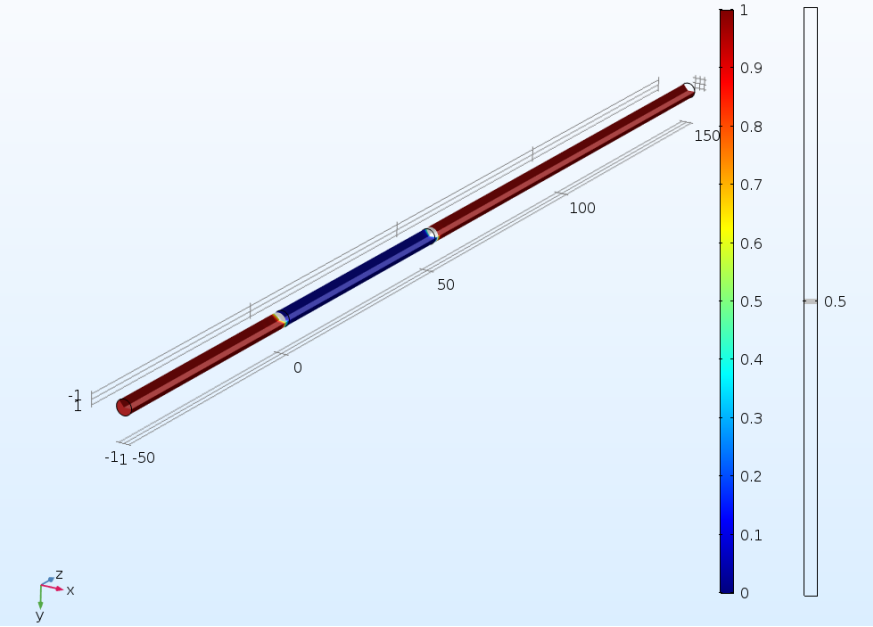

Figure 12. Model initialized with gaseous propane in red and liquid heptane in blue.

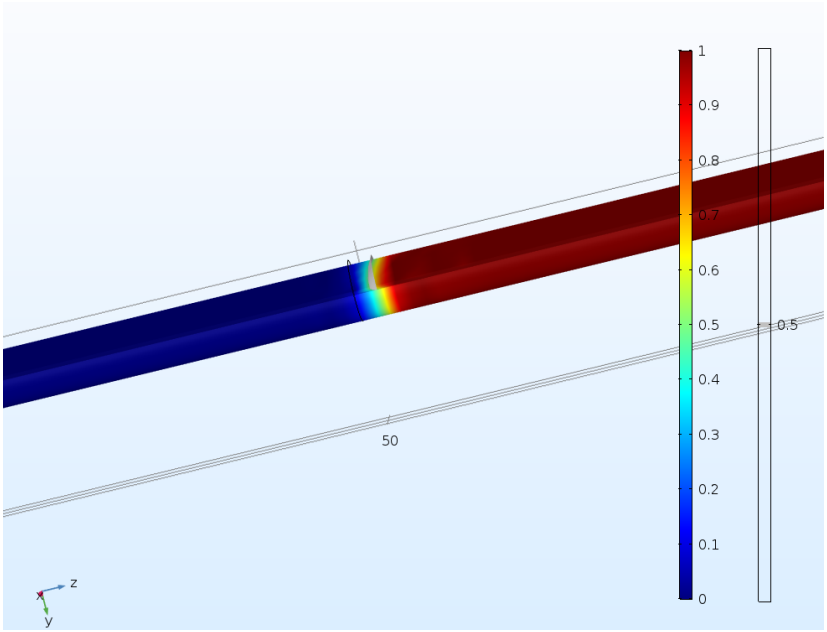

Figure 13. Model of interface with slight movement from initialized point due to non-equilibrium

4.1.3 Velocities under varying pressure gradients

As a control, the model was run with the inlet and outlet pressures equal to 100 psi, and the heptane phase was initialized with pressure equal to the inlet minus the expected capillary pressure, all calculated within COMSOL. Negligible movement was seen in the interface position after 0.05 seconds, which can be seen below in **Fig. 14**, which shows interface position at time 0 seconds on the left and 0.05 seconds on the right.

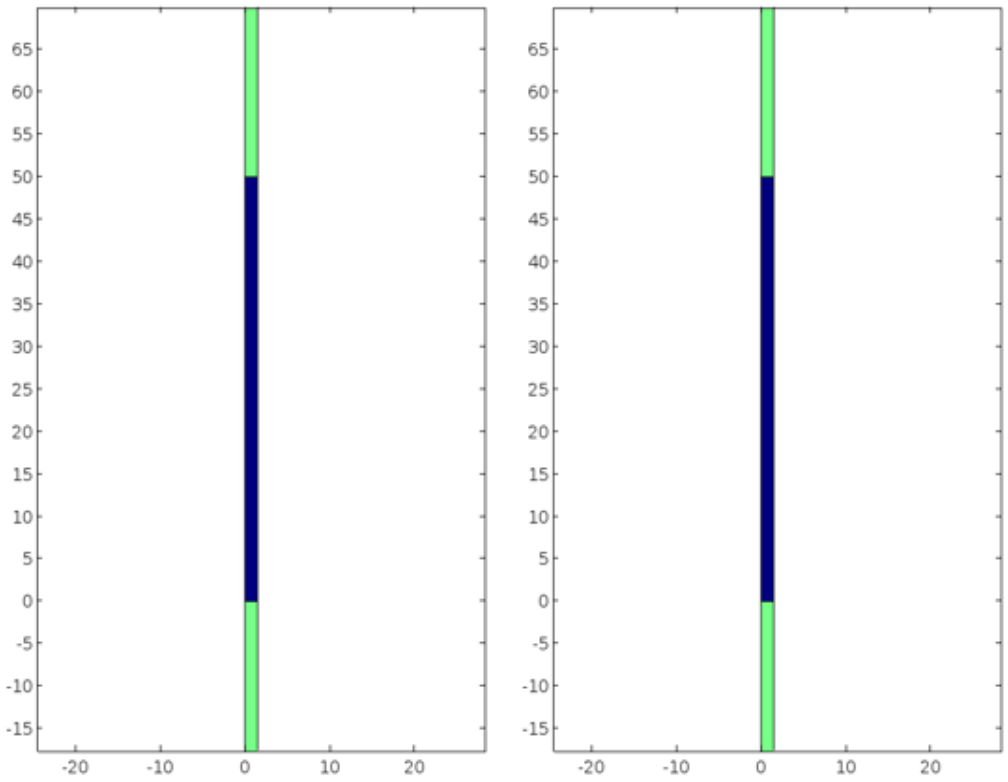

Figure 14. Interface position t = 0 and t = 0.05 seconds under no pressure gradient

To set a baseline for the additional contribution that acoustic waves have, effective pressure gradients of 2 psi/ft, 10 psi/ft, 30 psi/ft, and 50 psi/ft were evaluated with no acoustic interference. **Figures 15 through 18** show the movement of the interface from 0 to 0.05 seconds under these pressure gradients respectively.

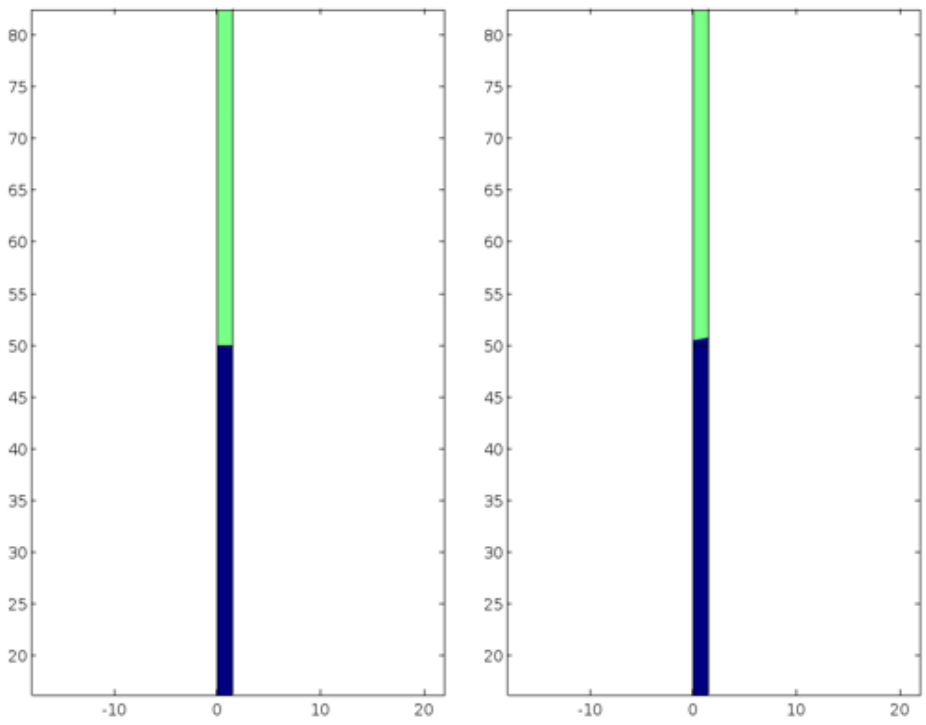

Figure 15. Interface position t = 0 and t = 0.05 seconds under pressure gradient of 2 psi/ft

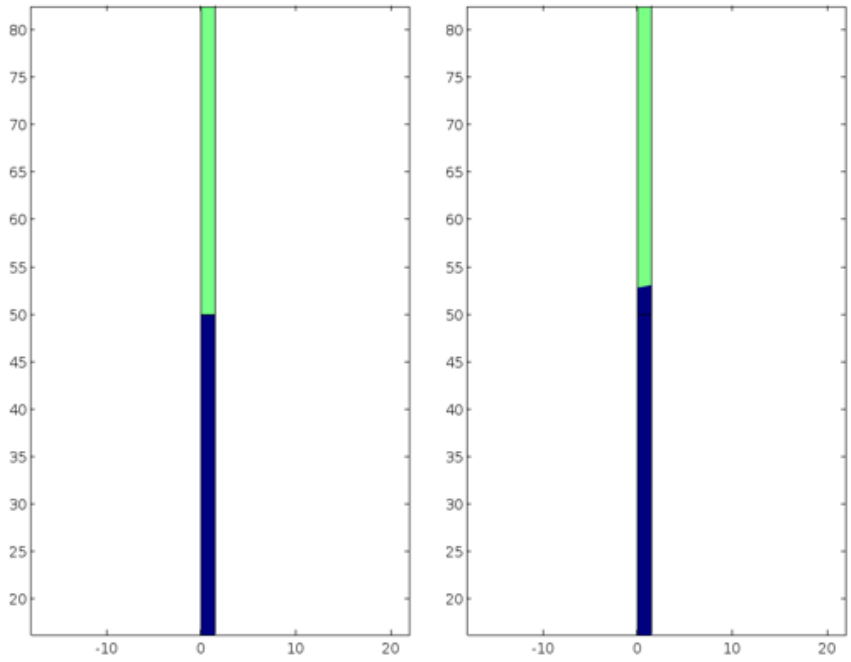

Figure 16. Interface position t = 0 and t = 0.05 seconds under pressure gradient of 10 psi/ft

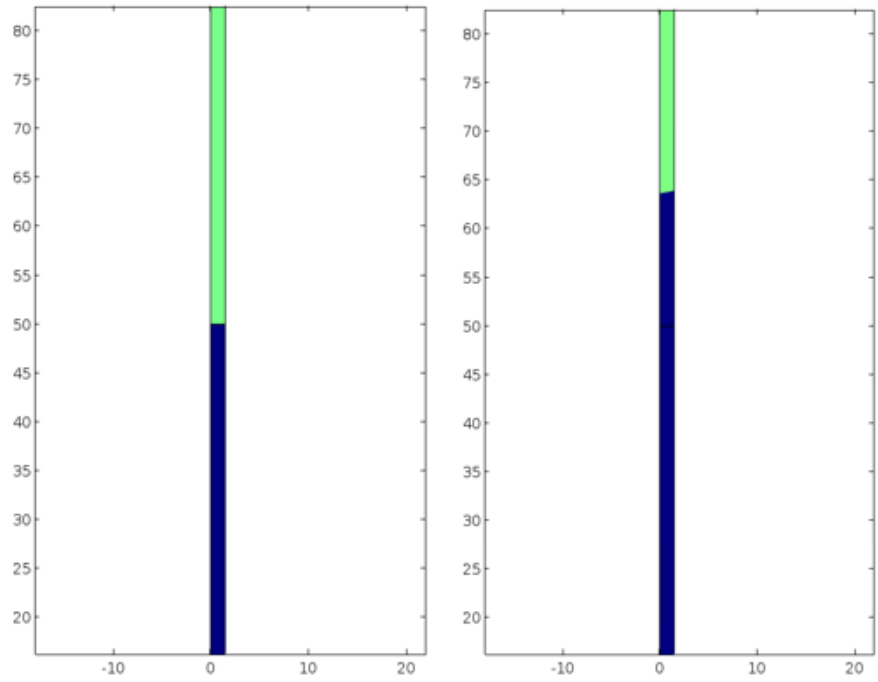

Figure 17. Interface position t = 0 and t = 0.05 seconds under pressure gradient of 30 psi/ft

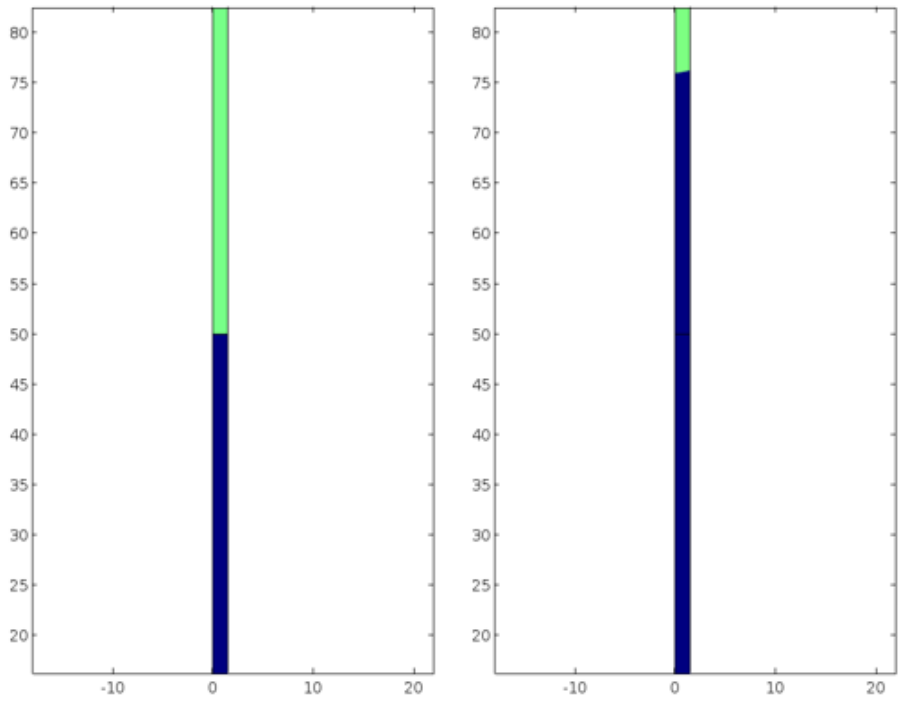

Figure 18. Interface position t = 0 and t = 0.05 seconds under pressure gradient of 40 psi/ft

The results from the four pressure gradients are summarized in **Table 1** below.

Table 1. Summary of interface movement under various pressure gradients.

Gradient	**Interface Displacement**	**Time**	**Velocity**
psi/ft.	μm	s	m/s
2	0.64	0.05	$1.28 \cdot 10^{-5}$
10	4.13	0.05	$8.26 \cdot 10^{-5}$
30	13.95	0.05	$2.79 \cdot 10^{-4}$
50	26.22	0.05	$5.24 \cdot 10^{-4}$

4.2 Effective Frequencies

4.2.1 Approximating likely frequencies

To get a better idea of what range of frequencies might be the most effective, the amplitude of interface displacement, which is correlated to wavelength through an assumed phase factor of zero, might be most reasonably effective within 1/10 to 2 times the radius of the capillary tube. Smaller wavelengths, which correspond to higher frequencies, might exhibit diminishing increases in net velocity with the time average of the displacement cycles. Displacements larger than twice the radius of the capillary tube might not be reasonable based on the energy required for displacement, especially because the interface is being displaced past a contact angle of 90 degrees. Because the radius of the capillary tube in the following simulations was 1.5 μm, the most effective wavelengths might reasonably be between 0.15 μm and 3 μm.

To translate these wavelengths to frequency approximations, **Eq. 4.6** was employed, with f being the frequency in Hz, c being the wave velocity in m/s, and λ being the wavelength in m.

$$f = \frac{c}{\lambda} \tag{4.6}$$

Although more accurate approximations of compressional wave velocities would be important to discerning exact frequencies, only general ranges are needed to find bounds for the simulation. A much more robust review of sound wave velocities through hydrocarbons is given by Tahani (2011), but they generally range as low as 200 m/s for propane and up to over 1300 m/s for heptane. The effect that this has on frequency approximations for the aforementioned wavelengths can be seen in **Table 2** below.

Table 2. Frequencies in MHz at varying compressional wave velocities

c, m/s	λ = 0.15 μm	λ = 3 μm
200	1,333	66.7
400	2,667	133
600	4,000	200
800	5,333	267
1,000	6,667	333
1,200	8,000	400
1,400	9,333	467

Although the spectrum of frequencies is quite large, much of it spans the MHz domain. This distinction will be discussed later, but it is important to note that much of the field successes and laboratory measurements were done in the kHz range, and that even the maximum wavelength corresponds to frequencies that are orders of magnitude greater than what is implemented.

4.2.2 Velocities under varying pressure gradients

Due to limitations in the modeling process, the acoustic waves were simulated as ambient pressure oscillations and not necessarily as waves being propagated from an acoustic source. This helped prevent interference between waves as well as disregarded attenuation across the length of the capillary tube. These pressure oscillations were

applied across both the propane the heptane phases, and the interface displacement was determined within COMSOL.

In order to evaluate the additional contribution that these compressional oscillations had on the capillary velocities, a range of frequencies covering those in **Table 3** were applied while the model was under a 10 psi/ft pressure gradient. Without the applied compressional waves, the displacement after 0.05 seconds for this pressure gradient was 4.67 μm. **Table 3** below shows the new displacements of the interface after the same 0.05 seconds at varying frequencies.

Table 3. Frequency dependent displacements after 0.05 seconds under a 10 psi/ft pressure gradient

Frequency	**Displacement**	**Relative Increase**
MHz	μm	%
100	4.13	0.0
500	4.18	1.1
1000	4.63	12.1
1500	4.66	12.9
1800	4.67	13.1
2000	4.67	13.1
3000	4.60	13.0
4000	4.52	11.5
5000	4.43	9.5
6000	4.29	7.2

The percentage increase in displacement at these frequencies was plotted below in **Fig. 19**. It can be seen that the maximum displacement occurred at around 1,800 MHz with the majority of increase occurring between about 750 MHz and 6,000 MHz.

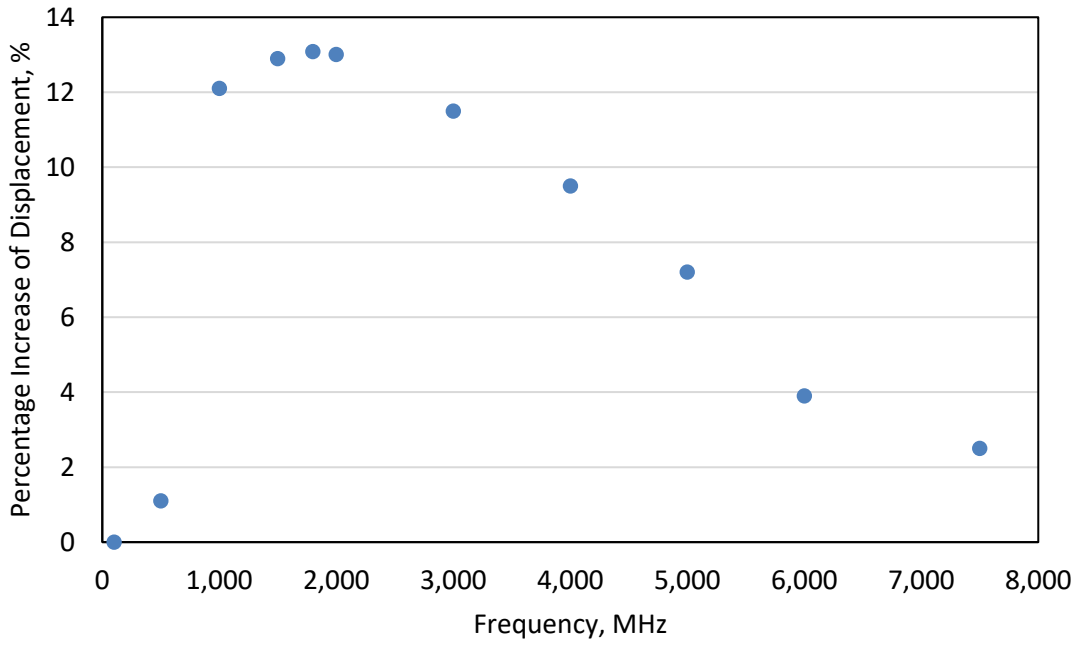

Figure 19. Percentage increase of interface displacement after 0.05 seconds at varying frequencies under a 10 psi/ft pressure gradient.

Assuming the other pressure gradients have similar distributions, the 1,800 MHz was then applied to the remaining 2 psi/ft, 30 psi/ft, and 50 psi/ft gradients respectively. The measured displacements after 0.05 seconds along with the magnitude and percentage increases from the base cases are recorded below in **Table 4**.

Table 4. Summary of interface displacements over 0.05 seconds with ambient pressure waves of 1,800 MHz

Gradient	**Displacement**	**ΔDisplacement**	**Percentage Increase**
psi/ft	μm	μm	%
2	0.76	0.12	18.75
10	4.67	0.54	13.08
30	15.07	1.12	8.03
50	27.65	1.43	5.45

Plotted in **Fig. 20** is the magnitude of interface displacement and the percentage increase under the 1,800 MHz ambient pressure oscillation. Although the magnitude of displacement is still increasing as the pressure gradient increases, it should be noted that the percentage contribution is decreasing. This would indicate that the increases in velocity with increasing pressure gradients are due mostly to the changes in pressure gradient instead of the contribution from the pressure oscillations.

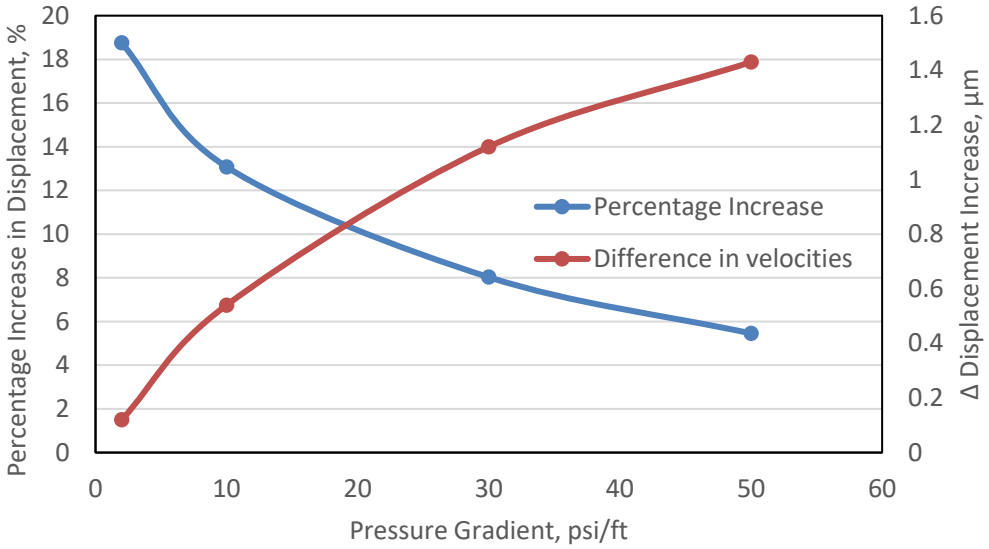

Figure 20. Magnitude of interface displacement (Red) and percentage increase of initial displacement (Blue) after 0.05 seconds in the presence of 1,800 MHz pressure waves.

Chapter 5: Conclusions and Future Work

5.1 Conclusions

Condensate banking is a problem that may severely hinder flow rate around the wellbore, which often leads to describing it as an added skin as well as decreasing the quality of the fluid stream at the surface. Many methods for preventing condensate banking have been proposed along with those to mitigate the negative effects once it has occurred. One such mitigating prospective is the use of acoustic stimulation. Based on the results developed from chapters 3 and 4, the following conclusions have been made.

- In general, there was increased displacement of the gas-liquid interface when in the presence of simulated compressional waves. For a pore radius of 1.5 μm, the majority of the effective frequencies was contained within approximately 750 MHz and 6,000 MHz with the maximum benefit achieved at an approximate frequency of 1,800 MHz.
- Although there is considerable increases in flow with larger pressure gradients, the relative contribution that acoustic waves have on moving the gas-liquid interface diminishes with larger ambient pressure gradients. This would indicate that the pressure gradient plays a more significant role in the interface velocity.
- Frequencies targeted specifically at affecting capillary pressures through cyclic interface displacement in micrometer-sized pores result in incredibly high frequencies that range from MHz to even GHz range. The attenuation increases dramatically as frequencies increase, and not many acoustic sources can attain sustained frequencies in these ranges.

- In terms of optimizing field treatments to remove condensate banking, or even to continue with cases targeted at increasing production during waterflooding, the other competing mechanisms described in chapter 2.4.2 should be explored as controlling factors.

References

Aarts, A., & Ooms, G. 1998. Net flow of compressible viscous liquids induced by travelling waves in porous media. *Journal of Engineering Mathematics* **34**(4): 435-450. https://doi.org/10.1023/A:1004314014329

Aarts, A., Ooms, G., Bil, K., & Bot, E. 1999. Enhancement of Liquid Flow Through a Porous Medium by Ultrasonic Radiation. *SPE Journal* **4**(4): 321-327. SPE-57720-PA https://doi.org/10.2118/57720-PA

Abramov, V., Mullakaev, M., Abramova, A., Esipov, I., & Mason, T. 2013. Ultrasonic technology for enhanced oil recovery from failing oil wells and the equipment for its implemention. *Ultrasonic Sonochemistry* **20**(5): 1289-1295. https://doi.org/10.1016/j.ultsonch.2013.03.004

Alhomadhi, E., Amro, M., & Almobarky, M. 2014. Experimental application of ultrasound waves to improved oil recovery during waterflooding. *Journal of King Saud University - Engineering Sciences* **26**(1): 103-110. https://doi.org/10.1016/j.jksues.2013.04.002

Bonn, D., Eggers, J., Indekeu, J., Meunier, J., and Rolley, E. 2009. Wetting and spreading. *Reviews of Modern Physics*. **81**: 738-805. https://doi.org/10.1103/revmodphys.81.739

Comsol Inc. 2017. Capillary Filling - Level Set Method. Burlington, MA: COMSOL Multiphysics(2017 Revision), https://www.comsol.com/model/capillary-filling-phase-field-method-1878 (accessed 12 April 2017).

Coats, K., & Smart, G. 1986. Application of a Regression-Based EOS PVT Program to Laboratory Data. *SPE Reservoir Engineering* **1**(3): 277-299. SPE-11197-PA. https://doi.org/10.2118/11197-PA

Economides, M., Hill, D., Ehlig-Economides, C., & Zhu, D. 2016. Petroleum Production Systems (2 ed.). Prentice Hall.

Fan, L., Jamaluddin, B., Kamath, A., Mott, J., Pope, G., Shandrygin, A., & Whitson, C. 2005. Understanding Gas-Condensate Reservoirs. *Oilfield Review* **17**(4): 17-27. Schlumberger.

Ganiev, R., Ukrainskii, L., & Frolov, K. 1989. Wave mechanism for the acceleration of liquid flowing in capillaries and porous media. *Soviet Physics Doklady* **34**: 519.

Gregory, S., Maurice, L., West, J., & Goddy, D. 2014. Microbial communities in UK aquifers: Current understanding and future research needs. *Quarterly Journal of Engineering Geology and Hydrogeology*, **47**(2): 145-157. https://doi.org/10.1144/qjegh2013-059

Kouznetsov, O., Simkin, E., Chilingar, G., & Katz, S. 1998. Improved oil recovery by application of vibro-energy to waterflodded sandstones. *Journal of Petroleum Science and Engineering* **19**(3-4): 191-200. https://doi.org/10.1016/S0920-4105(97)00022-3

McCain, W. 1990. The Properties of Petroleum Fluids. Tulsa, OK: PennWell Books.

Mohammadian, E., Junin, R., Rahmani, O., & Idris, A. 2013. Effects of sonification radiation on oil recovery by ultrasonic waves stimulated water-flooding. *Ultrasonics* **53**(2): 607-614. https://doi.org/10.1016/j.ultras.2012.10.006

Naderi, K., & Babadagli, T. 2010. Influence of intensity and frequency of ultrasonic waves on capillary interaction and oil recovery from different rock types. *Ultrasonics Sonochemistry* **17**(3): 500-508. https://doi.org/10.1016/j.ultsonch.2009.10.022

Narayanaswamy, G., Pope, G., Sharma, M., Hwang, M., & Vaidya, R. 1999. Predicting Gas Condensate Well Productivity Using Capillary Number and Non-Darcy Effects. Presented at the SPE Reservoir Simulation Symposium, Houston, Texas, 14-17 Feburary. SPE-51910-MS. https://doi.org/10.2118/51910-MS

Niu, Q., Revil, A., & Saidian, M. 2016. Salinity dependence of the complex surface conductivity of the Portland sandstone. *GEOPHYSICS* **81**(2): D125-D140. https://doi.org/10.1190/geo2015-0426.1

O'Connell, R. and Budiansky, B. 1977. Viscoelastic Properties of Fluid-Saturated Cracked Solids. Journal of Geophysical Resarch **82**(36): 5719-5735. https://doi.org/10.1029/JB082i036p05719

Raghavan, R., Chun, W., & Jones, J. 1999. Practical Considerations in the Analysis of Gas-Condensate Well Tests. SPE Reservoir Evaluation & Engineering **2**(3): 288-295. SPE-56837-PA. https://doi.org/10.2118/56837-PA

Sayed, M., & Al-Muntasheri, G. 2016. Mitigating the Effects of Condensate Banking: A Critical Review. SPE Production & Operations **31**(2): 85-102. SPE-168153-PA. https://doi.org/10.2118/168153-PA

Sohrabi, M., & Jamiolahmady, M. 2009. Application of ultrasonic irradiation for well deliverability improvement in gas-condensate reservoirs. Journal of Petroleum

Science and Engineering **64**(1-4): 88-94. https://doi.org/10.1016/j.petrol.2008.12.007

Tahani, H. 2011. Determination of the Velocity of Sound in Reservoir Fluids Using an Equation of State. Dissertation, Heriot-Watt University, Edinburgh, United Kingdom (November 2011).

Yang, T., Ruhrgas, E., Christoffersen, K., & Ivarrud, E. 2007. LBC Viscosity Modeling of Gas Condensate to Heavy Oil. Presented at the SPE Annual Technical Conference and Exhibition, Anaheim, California, 11-14 November. SPE-109892-MS. https://doi.org/10.2118/109892-MS

Zhu, T., Huang, X., & Vajjha, P. 2005. Downhole Harmonic Vibration Oil-Displacement System: A New IOR Tool. Presented at the SPE Western Regional Meeting. Irvine, California, 30 March - 1 April. SPE-94001-MS. https://doi.org/10.2118/94001-MS

Appendix A: Nomenclature

d	Interface distance, m
F_{fr}	Frictional boundary force, N
F_{st}	Surface tension force, N
g	Gravity vector, m/s^2
I	Identity matrix, unitless
J	Productivity index, unitless
k	Wavenumber, and is equal to $\frac{2\pi}{\lambda}$, m^{-1}
P	Pressure, psi
P_c	Capillary pressure, psi
$P_{non\text{-}wet}$	Pressure of non-wetting fluid, psi
P_{res}	Reservoir Pressure, psi
P_{wet}	Pressure of wetting fluid, psi
P_{wf}	Wellbore pressure, psi
r	Radius of the meniscus, m
R	Capillary tube diameter, m
s	Skin, dimensionless
t	Time, sec
v	Interface velocity, m/s
u	Fluid velocity, m/s
β	Slip length, m
δ	Dirac delta function, unitless
ε	Thickness of the interface, m
γ_i	Parameter of initialization, usually set equal to largest magnitude of velocity, unitless
γ	Interfacial tension, dyne/cm
γ_{sl}	Solid-liquid interface, unitless
γ_{lg}	Liquid-gas interface, unitless
θ	Contact angle, degrees
λ	Wavelength, m

μ	Dynamic viscosity, Ns/m^2
ρ	Density, kg/m^3
σ	Surface tension coefficient, N/m
φ	Phase shift, unitless
ω	Frequency, Hz
ϕ	Phase representation ($\phi = 0$ for gas, $\phi = 1$ for liquid), unitless